Reusable polyacrylonitrile-sulfur extractor of heavy metal ions from wastewater

Peng Li[a, b], Haibin Jiang[b, c], Ariel Barr[b], Zhichu Ren[b], Rui Gao[b], Hua Wang[b], Weiwei Fan[b], Meifang Zhu[d], Guiyin Xu[b, d]*, Ju Li[b]*

[a] School of Environment Science and Spatial Informatics, China University of Mining and Technology, Xuzhou City, Jiangsu 221008, China

[b] Department of Nuclear Science and Engineering and Department of Materials Science and Engineering, Massachusetts Institute of Technology, Cambridge, MA 02139, USA

[c] SINOPEC Beijing Research Institute of Chemical Industry, Beijing 100013, China

[d] State Key Laboratory for Modification of Chemical Fibers and Polymer Materials, College of Materials Science and Engineering, Donghua University, Shanghai 201620, China

This is the author manuscript accepted for publication and has undergone full peer review but has not been through the copyediting, typesetting, pagination and proofreading process, which may lead to differences between this version and the Version of Record. Please cite this article as doi: 10.1002/adfm.202105845.

ABSTRACT: Mercury, lead, and cadmium are among the most toxic and carcinogenic heavy metal ions (HMIs), posing serious threats to sustainability of aquatic ecosystems and public health. There is an urgent need to remove these ions from water by a cheap but green process. Traditional methods have insufficient removal efficiency and reusability. Structurally robust, large surface-area adsorbents functionalized with high-selectivity affinity groups to HMIs are attractive filter materials. Here, we report an adsorbent prepared by vulcanization of polyacrylonitrile (PAN), a nitrogen-rich polymer, giving rise to PAN-S nanoparticles with cyclic π-conjugated backbone and electronic conductivity. PAN-S can be coated on ultra-robust melamine (ML) foam by simple dipping and drying. In agreement with hard/soft acid/base theory, N- and S-containing soft Lewis bases have strong binding to Hg^{2+}, Pb^{2+}, Cu^{2+}, and Cd^{2+}, with extraordinary capture efficiency and performance stability. Furthermore, the used filters, when collected and electrochemically biased in recycling bath, can release the HMIs into the bath and electrodeposit on the counter-electrode as metallic Hg^0, Pb^0, Cu^0, and Cd^0, and the PAN-S@ML filter can then be reused at least 6 times as new. The electronically conductive PAN-S@ML filter can be fabricated cheaply and holds promise for scaled-up applications.

Keywords: Soft Lewis acid; Electro-desorption; Metal recovery; Recycling; Drinking water filter

1 Introduction

Heavy metal ions (HMIs) discharged from industrial processes (e.g. mining, steel, battery, electronic circuit board production, leather tanning, electroplating) and waste runoffs pose serious challenges for aquatic ecosystem sustainability and public health. Mercury, lead, and cadmium HMIs are extremely toxic, causing severe adverse effects on humans such as cancer, birth defects, mental retardation, kidney damage, as well as DNA damage from even trace level (ppb or ppt) HMIs exposure.[1-3] Industries face increasingly strict regulations for wastewater disposal to reduce the environmental impact of HMIs.[4] But HMIs still regularly exist in the natural environment and drinking water sources, especially in less-developed regions.[5,6] Several technologies have been pursued for the

elimination of HMIs from polluted water, including chemical precipitation,[7,8] solvent extraction,[9,10] ion exchange,[11,12] and osmosis.[13] However, due to low removal efficiency, high treatment cost, and the production of secondary pollutions, considerable work remains to be done. Especially when treating wastewater with relatively low HMI concentrations (US EPA limits are 0.002 mg (Hg)/L, 0.000 mg (Pb)/L, 0.005 mg (Cd)/L for drinking water, or equivalently 2 ppb (Hg), 0 ppb (Pb) and 5 ppb (Cd)), the cost-efficacy envelope is often disappointing. Adsorption can have high uptake capacity, good selectivity, and fast kinetics, and thus provides a promising mechanism for HMIs decontamination.[14,15] Adsorbents that have been functionalized with matching metal-ion affinity groups and robust operation conditions (i.e. no stringent pH or post-processing requirements) are prerequisites. Hg^{2+}, Pb^{2+}, Cu^{2+}, and Cd^{2+} are Lewis soft acids, and possess stronger-binding compatibility with Lewis soft base groups e.g. RNC, R_2S, RSH, and RS^-, according to the hard/soft acid/base (HSAB) theory.[16] Based on this, nitrogen and sulfur-containing groups have been incorporated into organic/inorganic frameworks for Hg^{2+}, Pb^{2+}, Cu^{2+}, and Cd^{2+} metal ion removal.[17-23] The inorganic adsorbents, mainly amine-rich functionalized carbon material and metal sulfides, can be facilely synthesized and display high uptake capacity in the adsorption of these HMIs.[24-27] However, the deficiencies of low adsorption pH value, formation of H_2S gas, and the dissolution of active components restrict its widespread utilization. Among the organic adsorbents, thiol/thioether/pyridyl-based covalent/metal-organic frameworks show high uptake capacity for Hg^{2+}, Pb^{2+}, Cu^{2+}, and Cd^{2+} adsorption.[28-33] But due to high preparation cost, deterioration from pH corrosion, and inferior stability for reuse, thiol (-SH) containing COF or MOF are essentially unused in any practical wastewater treatment. Polymer-based adsorbents derived from in-situ anchoring of exogenous Lewis basic sites show comparative ease in preparation and fine control of the adsorbent structure.[34-37] The reported *D*-limonene, canola oil, and dicyclopentadience inverse vulcanized S-containing adsorbents have displayed easy preparation, large Hg^{2+} adsorption capacity, and tonne scale production.[38,39] However, it also shows poor desorption and recycling performance because of

the strong affinity of the ionic bond formed between the heavy metal ions and the Lewis base sites. Desorption is the reversal of adsorption, so strong adsorption is typically accompanied by insignificant desorption, necessitating a compromise between adsorption and desorption (if no voltage bias) for applications, and this lack of reusability increases the lifecycle cost of filtration. Unfortunately, relatively little attention has been dedicated to the desorption of heavy metal ions, which leads to inferior reusability of the prepared adsorbents. Nanoscale adsorbent has been widely studied and pursued to obtain enlarged interfaces. The granulation or immobilization of the nanoparticle adsorbent will also be important for practical applications.

In this work, we report a highly porous, exceptionally stable, and easy-to-scale-up adsorbent grafted on industrially produced melamine foam, and a corresponding electro-desorption method for the elimination and recovery of multiple metal ions from wastewater. The melamine (ML) foam consists of open-cell polymer fibers, and serves as support for PAN-S nanoparticles that are the active component in water filtration. The endogenous Lewis basic C-N, C=N, and exogenous C-S-S-C sites were generated through a simple thermal polymerization between polyacrylonitrile (PAN) and sulfur (S) powder. Interestingly, HMIs adsorption on PAN-S surface is selective, enabling the separation of Hg^{2+}, Pb^{2+}, Cu^{2+}, and Cd^{2+} from the other metal ions. More importantly, the polymeric PAN-S nanoparticle can be stably fastened onto the skeleton of melamine sponge, which can withstand the filtration flow of HMI-containing water. After adsorption, the used sponges can be collected from various sites and moved to a central recycling bath, where the chemically adsorbed Hg^{2+}, Pb^{2+}, Cu^{2+}, and Cd^{2+} metals can be electrochemically desorbed, and reduced on the counter-electrode as metallic Hg^{0}, Pb^{0}, Cu^{0}, and Cd^{0} using electro-deposition, achieving the highest possible waste concentration. Both the adsorption and desorption processes are exceptionally robust, with almost no runoff or performance degradation over 6 adsorption-desorption cycles. This decentralized absorption but centralized recycling and electrodeposition paradigm can greatly reduce the cost for drinking water detoxification (Fig. 1).

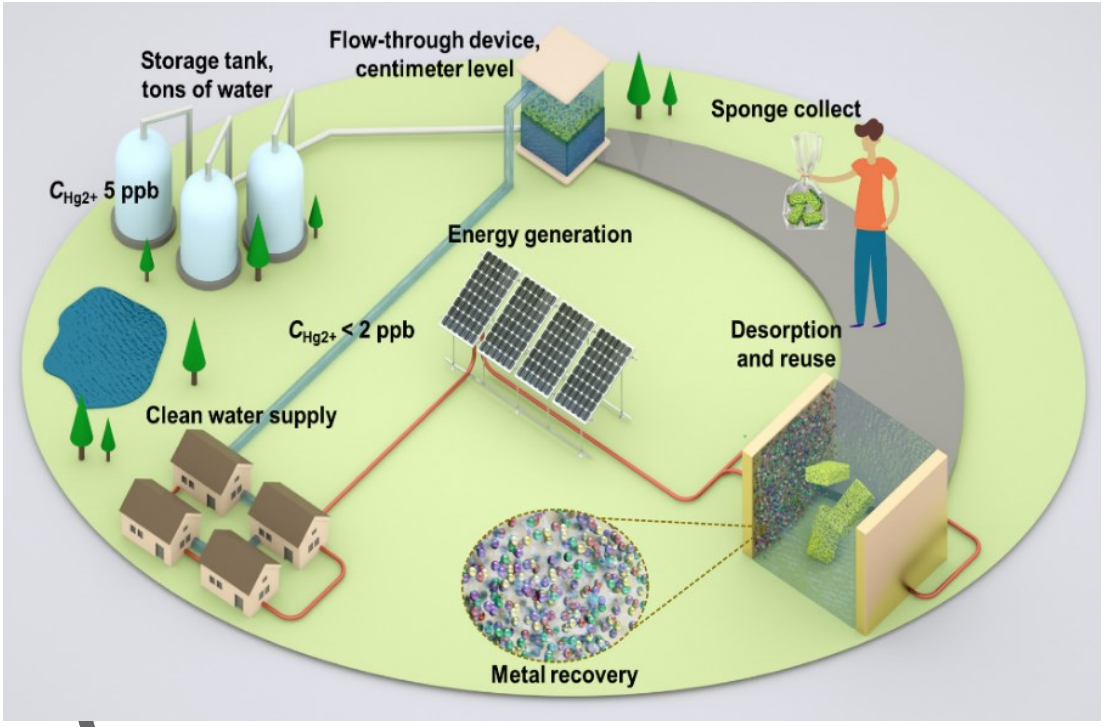

Fig. 1 Schematic demonstrating the HMIs polluted drinking water sources treatment and HMIs recovery with the proposed adsorption and electro-desorption method. First, tons of polluted water was drawn and stored as drinking water resource, a centimeter-level flow-through device packed with the fabricated PAN-S@ML sponge can in-situ intercept the toxic HMIs quickly and efficiently, and the pass-through water with the HMIs concentration below 1.0 EPA can be supplied to the village. Then the PAN-S@ML sponge can be collected and regenerated with intermittent renewable energy, e. g. solar photovoltaics. The PAN-S@ML sponge was desorbed with electro-desorption method along with the metal deposition in the cathode. The adsorbent can be reused, and the metal can be recovered simultaneously.

2 Results and Discussion

Preparation of PAN-S adsorbents and their metal ions affinity

PAN-S nanoparticles were fabricated by a thermal polymerization method using nitrogen-rich polymer PAN as the matrix precursor and S_8 powder as the S source (Fig. S1a). While pure PAN is an insulator, the sulfurized PAN gains cyclic conjugation as well sulfur chains grafted onto the polymer, which makes PAN-S electronically conductive, a feature well exploited in lithium-sulfur batteries.[40,41] The micromorphology and particle size of the prepared PAN-S powder is shown in Fig. 2a, and Fig. S1b indicates connecting and binding between the nanoscale PAN-S particles of average

size ~120 nm. The relatively low polymerization temperature ~300 ℃ permitted a reduced graphitization of the PAN substrate to prevent shrinkage and particle isolation[40]. The singly cross-linked PAN-S nanoparticles permit superior interface stability when used as adsorbent in an aqueous solution.

The HR-TEM images in Fig. S1c confirmed the agglomerated morphology and the nanoscale size of PAN-S particles. Poor crystallization of the PAN-S particles could be deduced from the irregular lattice diffraction. TEM-mapping images in Fig. 2a revealed uniform distribution of N and S on the PAN-S nanoparticle surface, which provide an abundance of active sites (e. g. C-N, C=N, and C-S-S-C) for metal ion adsorption. The mass ratio of C, N, O, and S elements reflected from the mapping results was appropriately 41:17:4:38. The XPS scanning spectra (Fig. S2a) of the PAN-S particle also showed that PAN-S mainly contains the elements C, N, O, and S, with a mass ratio of approximately 47:16:2:35, corroborating the TEM-mapping results. The XPS spectrum of high-resolution S scanning indicates confinement of S to C-S and S-S bonds (Fig. S2b). The binding energy peaks at 163.52 and 164.63 eV correspond to $S2p_{3/2}$ and $S2p_{1/2}$ orbitals in C-S bond, and the binding energy peaks at 161.68 and 162.79 eV signal the existence of $S2p_{3/2}$ and $S2p_{1/2}$ orbital in S-S bonds.[42,43] The C-S and S-S mass ratio calculated from the area in the high revolution S scanning spectra was 3.32:1. In the PAN-S structure, the C-S and S-S groups tend to form a C-S-S-C covalent bond, which promotes S anchor stability.[44-46]

The high-resolution XPS scanning for N1s indicates that N exists in the form of C=N and C-N groups, as demonstrated by binding energy peaks at 399.96 and 398.18 eV, respectively (Fig. S2c).[47,48] The binding state of the N atom well matched its chemical configuration in the reported PAN-S molecule.[47] The Raman spectroscopy of the as-prepared PAN-S nanoparticles is shown in Fig. S2d. The strong characteristic peaks at 181 and 805 cm^{-1} correspond to the C-S bond stretching, and the characteristic peaks at ~378 cm^{-1} are ascribed to in-plane bending of the C–S bond. The S-S bond can

be identified by the peaks at 926 and 1157 cm^{-1}, which are characteristic of the stretching of S-S bond containing rings, and the strong peaks at 1200 to 1600 cm^{-1} are characteristic of carbon-like materials obtained by pyrolyzing a polymer. Owing to the relatively low synthesis temperature, characteristic peaks for elemental sulfur or poly(sulfur) can be found at 472 cm^{-1}. The abundance of N and S bonds on the PAN-S nanoparticle surface provides an abundance of affinity sites for metal ions adsorption. [49-52]

The PAN-S nanoparticle displays outstanding affinity towards Hg^{2+}, Pb^{2+}, Cu^{2+}, and Cd^{2+} ions, with saturated adsorption capacity of 158.43, 120.68, 86.73, and 36.87 mg/g, at solution pH of 7.0, 5.0, 5.0, and 7.0, respectively (Fig. 2b). The uptake capacity of PAN-S was better than that of natural carbon, biomass, and synthetic clay adsorbents, though less than that of thiol (-SH) containing COF/MOF, and individual metal sulfide materials.[28, 39, 53,54] For example, MoS_2 and ZnS nanoparticles have superior reported saturated adsorption capacities of 340 and 2000 mg/g. [55,56] However, thiol (-SH) containing COF or MOF suffer from structural vulnerabilities, and have a narrow solution pH range for adsorption. In particular, Hg^{2+} is only adsorbed by the metal sulfide species under very acidic conditions (pH ~2.0-5.0), and generates H_2S off-gas during the adsorption process. Continuous leaching of metal ions from the adsorbent will also occur, which results in inferior process stability. From this standpoint, PAN-S has superior performance owing to a wide range of pH operating conditions and excellent stability. The adsorption behavior of Hg^{2+}, Pb^{2+}, Cu^{2+}, and Cd^{2+} metal ions on PAN-S nanoparticle surface can be well-fitted with the Freundlich model, indicating a chemically dominant interaction.

The effect of solution pH on metal ion removal efficiency was comprehensively explored, and the results are shown in Fig. 2c. The optimal solution pH for PAN-S metal ion uptake was appropriately 7.0, with uptake performance of Pb^{2+}, Cu^{2+}, and Cd^{2+} dramatically increased in comparison with more acidic or alkaline conditions. The maximum removal efficiency for Pb^{2+}, Cu^{2+}, and Cd^{2+} was 99.84%,

99.66%, and 93.55%, respectively. A high Hg^{2+} removal efficiency (>99.0%) was obtained in a broad solution pH range of 1.0 to 12.0, though the optimal adsorption still occurred at pH 7.0, where the removal efficiency reached 99.99%. This is ascribed to the saturate-coordinated N and S groups in PAN-S with an inferior affinity with H^+, thus the S-Hg^{2+} and N-Hg^{2+} ionic bond can break down the interaction between N, S and H^+. Furthermore, for the reason of the relative week affinity of N and S groups with Pb^{2+}, Cu^{2+}, and Cd^{2+} ions, the solution pH dependence adsorption trends become apparent. When the adsorption occurred in a mixture, the Hg^{2+}, Pb^{2+}, Cu^{2+}, and Cd^{2+} ions are preferentially adsorbed with K_d value 1666, 1653, 1631, and 1206, respectively. The K_d values of Hg^{2+}, Pb^{2+}, Cu^{2+}, and Cd^{2+} ions were much larger than those of Zn^{2+}, Ca^{2+}, Ni^{2+}, Mn^{2+}, Mg^{2+}, Fe^{3+}, and Al^{3+} species (detailed K_d values are listed in Table S1), which indicates that PAN-S nanoparticles capture Hg^{2+}, Pb^{2+}, Cu^{2+}, and Cd^{2+} ions with high selectivity when treated with mixture wastewater (Fig. 2d). The outstanding preferential affinity for Hg^{2+}, Pb^{2+}, Cu^{2+}, and Cd^{2+} ions can be ascribed to the N and S function groups on PAN-S surface which possess stronger affinity for soft Lewis acid HMIs. [57,58]

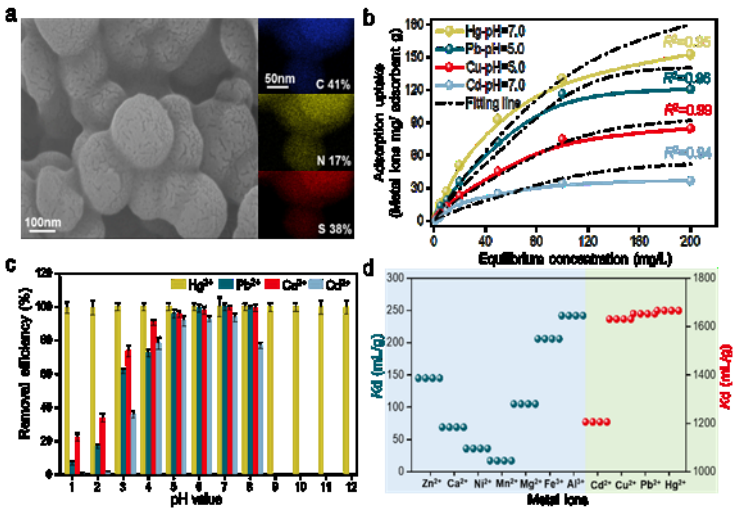

Fig. 2 SEM and TEM-mapping images and the corresponding mass content of the prepared PAN-S nanoparticles (**a**), adsorption capacities for Hg^{2+}, Pb^{2+}, Cu^{2+}, and Cd^{2+} (**b**), adsorption performance at different solution pH (**c**), and K_d values for various metal ions (**d**). Experimental condition: (b) PAN-S dosage 30.0 mg, volume of wastewater 50 mL, adsorption

duration 24 h, temperature 25 ℃; (c) Metal ions initial concentration 2.0 mg/L, PAN-S dosage 30.0 mg, volume of wastewater 50 mL, adsorption duration 2.0 h, temperature 25 ℃; (d) Initial concentration 0.1 mg/L, solution pH=5.0, PAN-S dosage 30.0 mg, volume of wastewater 50 mL, adsorption duration 2.0 h, temperature 25 ℃.

Preparation of PAN-S@ML sponge filter and their metal ions affinity

As structural support for the water filter, we use the open porous melamine foam ("Magic Eraser"). A very facile dipping and drying process into PAN-S ink can accomplish the synthesis of the PAN-S@ML sponge (Fig. S3). Due to the recyclability of N-methyl-pyrrolidinone (NMP) solvent, the process is cost-saving and sustainable. After the coating of PAN-S (with dilute polyvinylidene fluoride (PVDF) binder), the color of the white ML sponge changes to black. This indicates excellent coverage of PAN-S on the melamine skeleton (formaldehyde-melamine-sodium bisulfite copolymer) and electronic percolation. Interestingly, the PAN-S@ML filter (Fig. 3d) inherits the porosity and skeletal structure of the parent ML sponge. The SEM images indicate that PAN-S nanoparticles anchored onto the ML sponge skeleton structure while retaining rich pores structures at the same time. These pores structures provide abundant channels for wastewater flow-through in the sponge filter. It can be seen that the surface of the PAN-S@ML filter is covered with uniform nanoscale PAN-S particles. This unique structure promises good metal ion adsorption kinetics on the PAN-S@ML filter (Fig. 3e). The nitrogen adsorption-desorption isotherms and the pore size distribution of different sponge materials are displayed in Fig. S4. The BET surface area for the original sponge (Fig. S4a), PAN-S@ML filter, and PAN-S@ML filter after Hg^{2+} adsorption was 9.87, 9.64, and 7.98 m^2/g, respectively. This indicates that the BET surface area has not increased after PAN-S attachment. The pore size distribution shown in Fig. S4b indicates a decreased mesoporous structure after PAN-S attachment and metal ions adsorption. From the above, it can be deduced that a percolating PAN-S nanoparticles covered surface will be formed. The adsorption on the PAN-S@ML filter surface can be ascribed to the porous framework structure and exposed PAN-S nanoparticles.

A self-made adsorption device with PAN-S@ML filter as packing material was constructed, and a metal ion containing simulated wastewater batch treatment was conducted to evaluate the practicality of the proposed adsorption scheme, with results shown in Fig. 3. As shown in Fig. 3f, when high concentration Hg^{2+}, Pb^{2+}, Cu^{2+}, and Cd^{2+} metal ion containing wastewater was treated in the first cycle, the capture efficiency was as high as 100.0%, 100.0%, 99.48%, and 99.23%, respectively. For the subsequent 3 repetitions, high concentration Hg^{2+}, Pb^{2+}, Cu^{2+}, and Cd^{2+} metal ions containing wastewater can still be purified to meet EPA limit for drinking water within a very short 320 s duration (Fig. 3a, b, and c). The PAN-S nanoparticles provide an abundance of affinity sites for metal ion adsorption, which guarantees excellent HMI removal performance. Because a considerable percentage of the adsorbed metal ions are located on the surface of PAN-S@ML sponge, this platform provides a facile mechanism for the recycling of metal ions. The mass ratio of Cu on the PAN-S@ML filter surface reached 30.5% after 3 adsorption cycles (Fig. S5). As shown in Fig. S6, the mass ratio of Hg, Pb, and Cd on PAN-S@ML sponge surface after 3 adsorption repetitions was 26.2%, 34.3%, and 3.6%, respectively. The accumulated metal ions on PAN-S@ML filter surface have significant potential for separation and reuse.

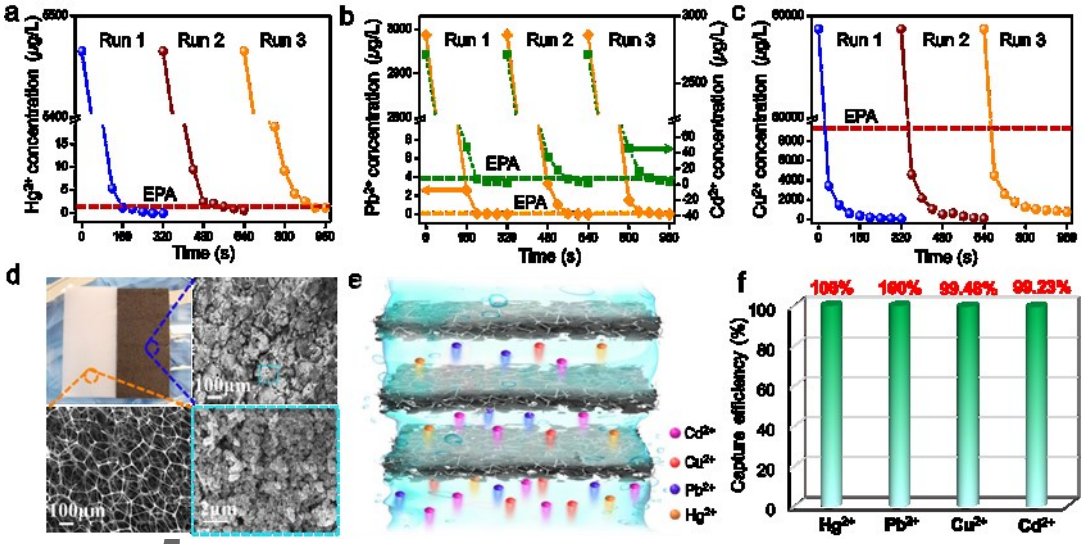

Fig. 3 Concentration of Hg^{2+} (**a**), Pb^{2+} and Cd^{2+} (**b**), and Cu^{2+} (**c**) during the flow-through adsorption, the digital photo and SEM images of pristine ML sponge and PAN-S@ML filter (**d**), the illustration for PAN-S@ML filter the flow-through adsorption method HMIs remove (**e**), and Hg^{2+}, Pb^{2+}, Cu^{2+}, Cd^{2+} capture efficiency in the flow-through adsorption (**f**). Experimental condition: Hg^{2+}, Pb^{2+}, Cu^{2+}, and Cd^{2+} initial concentration ~ 5.0 mg/L, 3.0 mg/L, 60.0 mg/L, and 3.0 mg/L, volume of the wastewater 300 mL, adsorption pH 7.0, 5.0, 5.0, and 7.0, repeated 3 times.

Zero-valent metal recycling

An electrochemical method was explored for the desorption of Hg^{2+}, Pb^{2+}, Cu^{2+}, and Cd^{2+} metal ions from the PAN-S@ML filter surface. The detailed illustration of the electrochemical desorption is presented in Fig. 4a. When a cell voltage (constant voltage 5.0 V) is applied, the N-metal and S-metal bonds formed between the PAN-S and HMIs will be broken due to electrolytic polarization. The desorbed Hg^{2+}, Pb^{2+}, Cu^{2+}, and Cd^{2+} metal ions will then be transmitted to the cathode and deposited as their corresponding zero-valent metallic form. A dilute 0.5 mol/L HNO_3 was used as electrolyte for the dissolution acceleration of Hg^{2+}, Pb^{2+}, Cu^{2+}, and Cd^{2+} metal ions. The current used during the electrochemical desorption was quite small (0.08 A), and therefore, only a small amount of electric power is required during the desorption. The adsorption-desorption treatment was continuously performed for 6 cycles, with amazing performance stability. An average capture efficiency for Hg^{2+}

was maintained at 97.72%, suffering only 2.28% attenuation in comparison with the first recycle at 100.0% (Fig. 4b).

The concentration of SO_3^{2-} and SO_4^{2-} in the electrolyte was monitored to understand the S runoff behavior during PAN-S@ML filter desorption, with results shown in Fig. 4c. The concentration of SO_3^{2-} and SO_4^{2-} in the electrolyte was low, even following 6 adsorption-desorption cycles, the outlet SO_3^{2-} and SO_4^{2-} was still only 0.319 and 0.027 mg/L. This is significantly below the 250 mg/L sulfate limit for States and public water systems. This result indicates that the S species in the PAN-S framework was stably anchored with almost no losses occurring during the electrocatalytic oxidation. Hence, a stable adsorption-desorption process for Hg^{2+}, Pb^{2+}, Cu^{2+}, and Cd^{2+} metal ions on the PAN-S@ML sponge can be realized. The mass content of Hg^{2+}, Pb^{2+}, Cu^{2+}, and Cd^{2+} metal ions on PAN-S@ML sponge decreases dramatically to a very low level of 3.9%, 1.6%, 2.3%, and 0.3% after the electrochemical recycling treatment (Fig. S6 and S7), indicating high desorption efficiency. Compared to the insignificant desorption performance obtained with direct 0.5 mol/L HNO_3 elution for PAN-S@ML sponge Cu^{2+} desorption, electro-desorption is an effective method to sperate HMIs from PAN-S@ML sponge surface (Fig. S8). The SEM images of the Ti cathode following the electrocatalytic desorption (Fig. 4d and Fig. S9) show that elemental Hg^0, Pb^0, Cu^0, and Cd^0 was obtained, which is the most compact and least hazardous waste form possible. Nevertheless, purifying catchment or tailings dam wastewater containing significant amounts of organic matter (such as humic matter) should be further explored.[59]

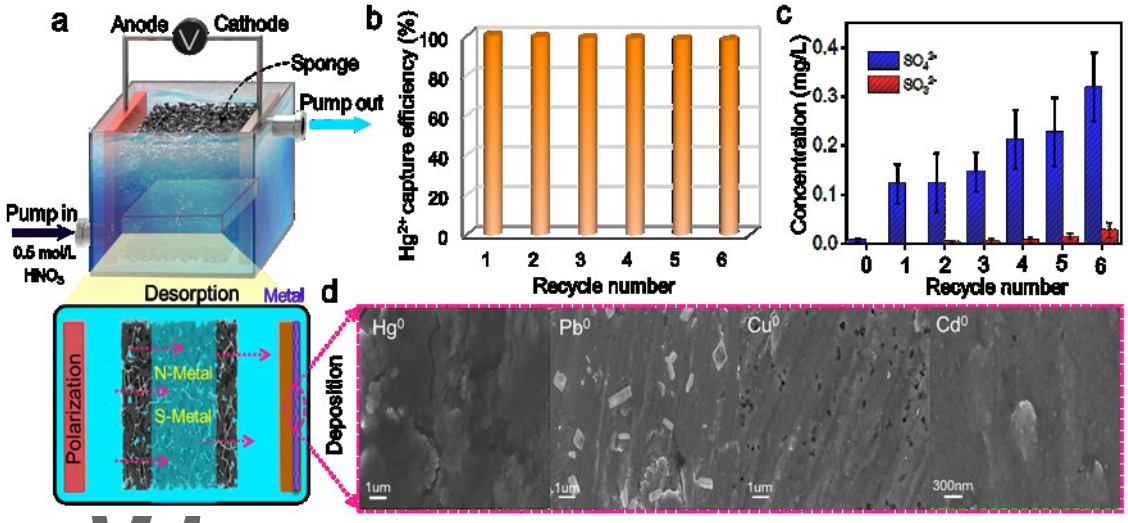

Fig. 4 Detailed illustration of electrocatalytic desorption (**a**), Hg^{2+} capture efficiency for the 6 cycles (**b**), the SO_3^{2-} and SO_4^{2-} concentration in the electrolyte (**c**), and Ti cathode surface after electro-desorption (**d**). Experimental condition: Hg^{2+}, Pb^{2+}, Cu^{2+}, and Cd^{2+} initial concentration ~ 5.0 mg/L, 3.0 mg/L, 60.0 mg/L, and 3.0 mg/L, volume of the wastewater 300 mL, adsorption pH 7.0, 5.0, 5.0, and 7.0, repeated 3 times. Adsorption-desorption cycle 6 times.

HMIs extraction mechanism

The extraction mechanism for Hg^{2+}, Pb^{2+}, Cu^{2+}, and Cd^{2+} metal ions from water solution with PAN-S adsorbents was explored with XPS analysis, Raman spectroscopy, and TEM mapping. From the XPS spectra after the Hg^{2+}, Pb^{2+}, Cu^{2+}, and Cd^{2+} adsorption, characteristic spectra for the metal species were observed (Fig. S10). Specifically, the Hg 4f at 100.81 eV, the Pb 4f at 138.19 eV, the Cu 2p at 932.02 eV, and the Cd 3d at 418.30 eV. And the surface accumulation of Hg^{2+}, Pb^{2+}, Cu^{2+}, and Cd^{2+} metal ions can be seen from the TEM mapping (Fig. 5d), which illustrates that metal ions were adsorbed and accumulated on the surface of the PAN-S nanoparticles. There are dramatic changes between the C-N, C=N, and -C-S-S-C- bonds before and after metal ion adsorption as described in XPS spectra, the details of which are shown in Fig. 5 and Fig. S11.

After Hg^{2+} adsorption, the binding energy peaks for C=N and C-N decreased from 399.96 eV and 398.18 eV to 399.69 eV and 397.84 eV, respectively, indicating the affinity between C=N, C-N and Hg^{2+}.[31,60-62] Compared with the C=N binding energy change (-0.27 eV), the C-N bond energy change

(-0.34 eV) was more significant, indicating that Hg^{2+} has a greater affinity for C-N bonds than C=N (Fig. 5a). The C-S-S-C group also experienced significant changes after Hg^{2+} accumulation, as shown in Fig. 5b. The binding energy peak of S $2p_{3/2}$ from the C-S bond and the binding peak of S $2p_{3/2}$ from the S-S bond (originally at 163.52 eV and 161.68 eV) greatly decreased, especially the peak of the S-S bond. The area of the binding energy peak shrank dramatically to around half that of pristine PAN-S, which can be ascribed to the breaking of S-S bonds during Hg^{2+} adsorption. The formation of S-Hg bonds can be identified from the S $2p_{3/2}$ and S $2p_{1/2}$ binding energy peak at 161.90 eV and 163.91 eV.[63] The affinity mechanism between PAN-S and Hg^{2+} can be described as occurring due to entrapment of Hg^{2+} by C=N, C-N, C-S, and S-S via electrostatic affinity, with S-S bond breakage resulting from stronger interaction between S and Hg^{2+} during adsorption.

The Hg^{2+}, Pb^{2+}, Cu^{2+}, and Cd^{2+} metal ions displayed different adsorption properties based on their interaction performance with PAN-S nanoparticles. For Pb^{2+} adsorption, the binding energy peaks for C=N and C-N at 399.96 eV and 398.18 eV decreased to 399.70 eV and 397.89 eV.[64, 65] The binding energy peak of S $2p_{3/2}$ belonging to C-S and S-S bonds decreased from 163.52 eV and 161.68 eV to 163.28 eV and 161.42 eV. An insignificant decrease in the binding energy peak for S-S bond was observed, which may indicate the affinity of S-Pb was not sufficient to break the S-S bond on PAN-S framework. For Cu^{2+} adsorption, change in the N 1s binding energy peak was also observed, decreasing from 399.96 eV and 398.18 eV to 399.89 eV and 398.12 eV.[66,67] Following Cd^{2+} adsorption, the binding energy peaks for C=N and C-N increased slightly to 400.08 eV and 398.27 eV, and the S-Cd bond can be found through S $2p_{3/2}$ and S $2p_{1/2}$ scanning at binding energy peaks of 161.80 eV and 162.78 eV.[68,69] This provides obvious evidence for Cd^{2+} adsorption by C=N, C-N, and C-S-S-C groups. Nevertheless, the C=N and C-N bond binding energy change was much smaller than for Hg^{2+}, Pb^{2+}, and Cu^{2+} adsorption. This can be ascribed to the relatively weak affinity between PAN-S and Cd^{2+} as compared with Hg^{2+}, Pb^{2+}, and Cu^{2+}.

The high-resolution XPS spectra for Hg 4f, Pb 4f, Cu 2p, and Cd 3d on the PAN-S surface is displayed in Fig. S10a. The Hg 4f binding energy yields two peaks from Hg $4f_{7/2}$ and Hg $4f_{5/2}$ at 100.81 eV and 104.86 eV, as expected from the initial Hg +2 state. The Hg $4f_{7/2}$ spectrum is a composite of two peaks with binding energy of 100.38 eV and 100.98 eV, while the Hg $4f_{5/2}$ spectrum can be divided into two distinct peaks 104.46 eV and 105.05 eV, which indicate the existence of N-Hg and S-Hg bonds, respectively[31]. The observed Hg atom binding energy states correspond to N and S bonded Hg, demonstrating that the C=N, C-N, and C-S-S-C functional groups have a strong affinity for Hg^{2+}. The Raman spectroscopy of the original PAN-S nanoparticle and after Hg^{2+}, Pb^{2+}, Cu^{2+}, and Cd^{2+} adsorption (Fig. 5c) showed that the C-S and S-S peak on PAN-S surface decrease obviously, which provides evidence of Hg^{2+}, Pb^{2+}, Cu^{2+}, and Cd^{2+} adsorption on PAN-S surface.

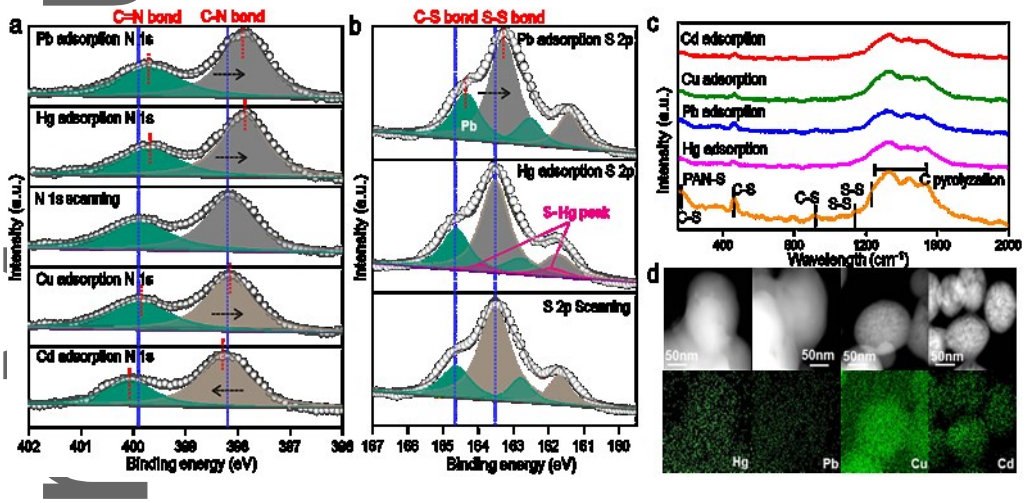

Fig. 5 High resolution XPS spectra of N 1s (**a**) and S 2p (**b**) before and after metal ions adsorption, Raman spectroscopy of original PAN-S nanoparticles and after Hg^{2+}, Pb^{2+}, Cu^{2+}, and Cd^{2+} adsorption (**c**), and TEM-mapping images of PAN-S nanoparticles after Hg^{2+}, Pb^{2+}, Cu^{2+}, and Cd^{2+} metal ion adsorption (**d**). Experimental condition: metal ions concentration 10.0 mg/L, pH=5.0, PAN-S dosage 30.0 mg, volume of wastewater 50 mL, adsorption duration 24.0 h, and temperature 25 ℃.

Based on the analysis above, the mechanism for Hg^{2+}, Pb^{2+}, Cu^{2+}, and Cd^{2+} metal ions adsorption with PAN-S nanoparticles can be deduced: the soft base groups of C-N, C=N, and C-S-S-C have a strong affinity with soft acid Hg^{2+}, Pb^{2+}, Cu^{2+}, and Cd^{2+} species. The proposed mechanism is

illustrated in Fig. S10c. The stronger the soft acid, the stronger the adsorption behavior; Hg^{2+} adsorption can also lead to the breakdown of S-S bonds in the C-S-S-C group.

Techno-economics and environmental sustainability

The components for PAN-S@ML sponge filter production are green and cost efficient. Cumulative economic demand and environmental sustainability were analyzed to evaluate the potential scalability of the proposed adsorption and electro-desorption method. The amount of PAN-S nanoparticle for one batch packing was 8.0 g, and the corresponding cost for the preparation of PAN-S and PAN-S@ML sponge, the cost of the electrodes, and electricity costs were all calculated and the total cost was 30.37 US $. The detailed cost was listed in Table S2. Besides, in consideration of the recycling possibility of NMP, the cost will be reduced in practical production. The initial Hg^{2+}, Pb^{2+}, Cu^{2+}, and Cd^{2+} concentration of the scattered drinking water intake point for the rural villages was assumed to be 5, 5, 10, and 1500 ppb, and the discharge standard was 2, 0, 5, and 1300 ppb, respectively. The treatment cost of the Hg^{2+}, Pb^{2+}, Cu^{2+}, and Cd^{2+} contaminated surface/groundwater was 0.17, 0.47, 0.94, and 0.94 US $/ton, which was low and competitive with the currently applied techniques (displayed in Fig. S12). These calculations prove the economic and environmental feasibility of the proposed adsorption and electro-desorption method for HMIs elimination and recovery.

3 Conclusion

In this work, we have demonstrated a sustainable, affordable, and easily implemented adsorbent preparation, as well as an ultra-robust and stable electrochemical recycling strategy for the highly efficient removal and recovery of Hg^{2+}, Pb^{2+}, Cu^{2+}, and Cd^{2+} from wastewater. Our approach involves the in-situ generation of endogenous Lewis basic C-N, C=N, and C-S-S-C affinity sites on PAN-S nanoparticle and the immobilization of the prepared nanoparticle adsorbent on a mechanically robust melamine foam. A simple thermal polymerization between polyacrylonitrile and sulfur powder were

introduced for the preparation of PAN-S nanoparticle, which displayed extensive pH (1.0~12.0) competence for Hg^{2+} adsorption and selective adsorption for Hg^{2+}, Pb^{2+}, Cu^{2+}, and Cd^{2+} HMIs. A facile dipping and drying process could accomplish the stably fasten PAN-S onto the skeletal surface of melamine sponge, the fabricated PAN-S@ML filter then inherited the porosity of ML sponge permitting the flow-through of wastewater and interception of the HMIs with the exposed affinity sites. The capture efficiency for Hg^{2+}, Pb^{2+}, Cu^{2+}, and Cd^{2+} containing wastewater with initial concentration of 5.0, 3.0, 60.0, and 3.0 mg/L was measured to be 100.0%, 100.0%, 99.48%, and 99.23%, and the outlet are all met the US EPA requirement for drinking, with very low sulfur runoff. And the mass ratio of the accumulated Hg^{2+}, Pb^{2+}, Cu^{2+}, and Cd^{2+} on the PAN-S@ML filter was as high as 26.2%, 34.3%, 3.6%, and 30.5%, respectively, indicating excellent usage of affinity sites. The HMIs can be collected from the wastewater and accumulated for significant recovery. Importantly, the PAN-S@ML filter could be regenerated with an electrocatalytic desorption method, and metallic states of Hg^0, Pb^0, Cu^0, and Cd^0 covered the surface of the counter electrode. Both the adsorption and desorption were exceptionally stable with nearly no attenuation after 6 cycles. The components for PAN-S@ML sponge production are green and cost effective, which offer a sustainable and affordable approach to the recovery of HMIs from wastewater and opens a promising avenue towards drinking water treatment.

4 Experimental Section

PAN-S nanoparticle preparation: In a typical synthesis of the PAN-S nanoparticles, 6.0 g polyacrylonitrile (PAN, Sigma-Aldrich, USA) and 24.0 g sulfur powder (Sigma-Aldrich, USA) are mixed and ground together. The powder is then sintered under argon atmosphere following a three-step thermal treatment procedure of: (1) heating from 20 to 300 ℃ at a constant heating rate of 3.0 ℃/min, (2) maintain temperature at 300 ℃ for 10 h, (3) cool from 300 ℃ to room temperature at a

constant cooling rate of 3.0 ℃/min. The as-prepared carbon polymer is then fully ground to obtain decentralized nanoparticles. The yield of PAN-S nanoparticles is 28.3%.

PAN-S@ML sponge filter fabrication: For the fabrication of the PAN-S@ML sponge filter, 0.8 g polyvinylidene fluoride (PVDF, Sigma-Aldrich, USA) was dissolved in 80 g N-methyl-pyrrolidinone (NMP, Sigma-Aldrich, USA) with vigorous stirring for 4.0 h at a constant temperature of 80 ℃. After cooling to room temperature, PAN-S nanoparticles (8.0 g) were added to the NMP solution and dispersed as a black-crosslinking slurry. Then the commercial ML foam (with exterior size of 60.0× 20.0×2.0 mm) is dipped into the slurry for 2.0 min, and air-dried to constant weight at 60 ℃ in oven.

Bulk metallic wastewater adsorption: The Hg^{2+}, Pb^{2+}, Cu^{2+}, and Cd^{2+} adsorption capacity of the as-prepared PAN-S nanoparticles and PAN-S@ML sponge was comprehensively investigated. The optimum solution pH, selective affinities for Hg^{2+}, Pb^{2+}, Cu^{2+}, and Cd^{2+} ions, and corresponding saturated adsorption capacities (q) were obtained for PAN-S nanoparticles. Systematic flow-through experiments were conducted using a self-designed device (Fig. S13a) packed with PAN-S@ML sponge, and high metal ion concentration (5.0 mg/L of Hg^{2+}, 3.0 mg/L of each Pb^{2+} and Cd^{2+}, and 60.0 mg/L of Cu^{2+}).

Feasibility of metal ion recovery from the PAN-S@ML sponge was explored using an electrolytic-desorption process with 150 mL 0.5 mol/L HNO_3 as electrolyte (Fig. S13b). Operational details of the experimental wastewater treatment and ion recovery method are shown in Fig. S1. The optimum solution pH for Hg^{2+}, Pb^{2+}, Cu^{2+}, and Cd^{2+} ion adsorption was investigated using 2.0 mg/L initial ion concentration, a 30 mg PAN-S nanoparticle dosage added to 50 mL simulated wastewater, and 2.0 h adsorption duration at 25 ℃ in a water bath shaker. For Hg^{2+}, controlled investigation of pH-dependent adsorption was conducted for the pH range 1.0 to 12.0 in increments of 1.0. Similarly, for Pb^{2+}, Cu^{2+}, and Cd^{2+}, the pH range 1.0 to 8.0 was investigated in increments 1.0.

Wastewater containing various metal ions, including Hg^{2+}, Pb^{2+}, Cu^{2+}, Cd^{2+}, Zn^{2+}, Ca^{2+}, Ni^{2+}, Mn^{2+}, Mg^{2+}, Fe^{3+}, and Al^{3+}, was used to evaluate selective affinity for Hg^{2+}, Pb^{2+}, Cu^{2+}, and Cd^{2+} ions. The solution pH was controlled to be 5.0, and initial concentration of each ionic species maintained at 100.0 μg/L. The mixture is set aside for 24 h, then passed through a 0.22 μm filter membrane. The result of this process is then treated as the initial solution in the adsorption experiments. For the adsorption experiments, a 30 mg dosage of PAN-S nanoparticles was added to 50 mL of simulated wastewater for a duration of 2.0 h at 25 ℃ in a water bath shaker. The affinity of PAN-S particles towards heavy metal ions can be expressed in terms of the distribution coefficient (K_d, mL/g) as given by the following equation:

$$K_d = \frac{c_0 - c_e}{c_e}\left(\frac{V}{M}\right) \quad (1)$$

where c_0 and c_e are the initial and terminal metal ions concentrations, mg/L; V the total volume of the solution, mL; and M the mass of the added PAN-S nanoparticles, g.

The saturated adsorption capacity (q) of PAN-S nanoparticles for Hg^{2+}, Pb^{2+}, Cu^{2+}, and Cd^{2+} ions were investigated using initial metal ion concentration wastewater prepared as 1.0, 2.0, 3.0, 4.0, 5.0, 10.0, 20.0, 50.0, 100.0, and 500.0 mg/L. It is worth noting that the solution pH was controlled at different values for Hg^{2+}, Pb^{2+}, Cu^{2+}, and Cd^{2+} adsorption because the ions have different pH-dependent dissociation properties. The solution pH used for Hg^{2+}, Pb^{2+}, Cu^{2+}, and Cd^{2+} q measurements was 7.0, 5.0, 5.0, and 7.0, respectively, where the q value has been calculated using the following equation:

$$q = \frac{(c_0 - c_e) \times V}{M} \quad (2)$$

Systematic flow-through treatment with metal ion recovery experiments were conducted to evaluate the applicability of the proposed scheme. The self-designed flow-through adsorption and

electrolytic-desorption devices were prepared with 3D-printed parts using polylactic acid plastics (PLA). The as-prepared PAN-S@ML sponge was employed as filling material to fabricate a flow-through adsorption device for the efficient treatment of high metal ion concentration wastewater with initial Hg^{2+} concentration 5.0 mg/L, Pb^{2+} and Cd^{2+} 3.0 mg/L, and Cu^{2+} 60.0 mg/L using 300.0 mL solution volume. Flow-through treatment was conducted 3 times under the same experimental conditions. The concentration of different metal ions was determined with inductively coupled plasma mass spectrometry (ICP-MS, Agilent 7900, USA). And the highest standard solution for Hg^{2+} detection was 200 ppb. It is worth noting that on account of the precipitation phenomenon that occurs in high metal ion concentration solutions, control of pH in the flow-through device is vital. To that end, the species distribution of Hg^{2+}, Pb^{2+}, Cu^{2+}, and Cd^{2+}as a function of pH was calculated using the software Visual MINTEQ ver 3.1, assuming an ionic strength of 0.2 mol/L, and NO_3^-concentration of 0.05 mol/L, with results shown in Fig. S14. Based on the results from the species distribution simulation, the controlled pH values for Hg^{2+}, Pb^{2+}, Cu^{2+}, and Cd^{2+} flow-through adsorption were 7.0, 5.0, 5.0, and 7.0, respectively.

Metal ion recovery: Regeneration of the PAN-S@ML sponge filter was conducted using an electrochemical process in a self-designed PLA reactor. In this process, the used PAN-S@ML sponge was packed in-between the electrodes, where graphite and titanium plate served as anode and cathode, respectively. The size of the electrode was 60.0 mm × 60.0 mm × 2.0 mm, and the distance between anode and cathode was 25.0 mm. The desorption treatment employed 150 mL of 0.5 mol/L concentration nitric acid as the electrolyte, with voltage of 5.0 V, for a duration of 0.5 h. After treatment, 0.15 mL of formaldehyde and 2.0 mL of 0.1 mol/L ethylenediaminetetraacetic acid was added to the electrolyte solution, and ion chromatography (IC, Thermo ICS-2100, UAS, with AS11-HC anion column) was employed to measure concentrations of SO_3^{2-} and SO_4^{2-}.

Material characterization: The morphology and the element distribution of the PAN-S nanoparticle and PAN-S@ML filter before and after ion adsorption was observed by field emission scanning electron microscopy (FE-SEM, ZEISS SUPRA 40, Germanely), high-resolution transmission electron microscopy (HR-TEM, Tecnai G2 F20, FEI, USA), and X-Ray energy dispersive spectroscopy (EDS-Mapping, SuperX, FEI, USA). The specific surface area of the synthetic PAN-S@ML sponge was determined according to the Brunauer-Emmett-Teller (BET) model and the pore size distribution was calculated via the Barrett-Joyner-Halenda (BJH) method using a micromeritics TriStar II Plus surface area analyzer (Micro, ASAP 2020, USA). The lattice structure, phase composition, and surface groups were recorded using X-ray diff raction (XRD, Bruker D8, Germany), and Fourier transform infrared spectroscopy (FT-IR, Nicolet-460, USA), with changes in the chemical and electronic states of N, S, and metal atoms detected using X-ray photoelectron spectroscopy (XPS, K-Alpha, USA). The cathode (Ti plate) before and after the electrolytic-desorption process was comprehensively characterized using FE-SEM and EDS-Mapping methods.

Data availability.

Data are available on reasonable request from the authors, according to their contributions.

Acknowledgments.

We would like to acknowledge support by Yintai Investment Co. LLC.

Reference

1 Y. Chen, M. J. Xu, J. Y. Wen, Y. Wan, Q. F. Zhao, X. Cao, Y. Ding, Z. L. Wang, H. X. Li, Z. F. Bian, *Nat. Sustain.*, 2021, **3**, 1.

2 B. Y. Li, Y. M. Zhang, D. X. Ma, Z. Shi, S. Q. Ma, *Nat. Commun.*2014, **5**, 1.

3 A. Joy, A. Qureshi, *Environ. Sci. Technol.* 2020, **54**, 14139.

4 World Health Organization. Drinking-Water Fact-Sheet. http://www.who.int/mediacentre/fact-sheets/fs391/en/.

5 The hindu center of politics and public policy. Heavy metals contaminating India's rivers: Samples from 65% of testing sites unsafe: survey. https://www.thehindu.com/news/national/heavy-metals-contaminating-indias-rivers/article30279681.ece, 2019.

6 UN environment programme. The Caribbean Environment Programme (CEP). Global versus Caribbean Studies on Mercury, Lead and Cadmium. https://www.unep.org/cep/heavy-metals, 2021.

7 X. Vecino, M. Reig, J. López, C. Valderrama, J. L. Cortina, *J. Environ. Manage.* 2021, **283**, 112004.

8 H. Y. Wu, W. J. Wang, Y. F. Huang, G. H. Han, S. Z. Yang, S. P. Su, H. Sana, W. J. Peng, Y. J. Cao, J. T. Liu, *J. Hazard. Mater.* 2019, **371**, 592.

9 J. M. Nan, D. M. Han, X. X. Zuo, *J. Power Sources* 2005, **152**, 278.

10 M. C. Aragoni, M. Arac, A. Bencini, S. Biagini, A. J. Blake, C. Caltagirone, F. Demartin, F. G. De, F. A. Devillanova, A. Garau, *Inorg. Chem.* 2008, **47**, 8391.

11 P. Goyal, C. S. Tiwary, S. K. Misra, *J. Environ Manage.* 2021, **277**, 111469.

12 Y. Ibrahim, V. Naddeo, F. Banat, S. W. Hasan, *Sep. Purif. Technol.*2020, **250**, 117250.

13 M. L. He, L. Wang, Y. T. Lv, X. D. Wang, J. N. Zhu, Y. Zhang, T. T. Liu, *Chem. Eng. J.* 2020, **389**, 124452.

14 K. Gai., A. Avellan, T. P. Hoelen, F. L. Linares, E. S. Hatakeyama, G. V. Lowry, *Water Res.* 2019, **157**, 600.

15 C. C. Long, X. Li, Z. X. Jiang, P. Zhang, Z. H. Qing, T. P. Qing, B. Feng. *J. Hazard. Mater.* 2021, **413** 125470.

16 Pearson, R. G. Chemical hardness. *Wiley-Vch, Verlag GmbH, Weinheim* (1997).

17 D. T. Sun, L. Peng, W. S. Reeder, S. M. Moosavi, D. Tiana, D. K. Britt, E. Oveisi, W. L. Queen. *ACS Cent. Sci.* 2018, **4**, 349.

18 J. P. Yang, Q. Li, M. Li, W. B. Zhu, Z. Q. Yang, W. Q. Qu, Y. C. Hu, H. L. Li, *Environ. Sci. Technol.* 2020, **54**, 2022.

19 L. M.Bofi, S. Royuela, F. Zamora, M. L. R. González, J. L. Segura, R. M. Olivas, M. J. Mancheño, *J. Mater. Chem. A* 2017, **5**, 17973.

20 J. T. Wang, Y. W. Hong, Z. C. Lin, C. L. Zhu, J. Da, G. H. Chen, F. Jiang, *Water Res.* 2019, **160**, 288.

21 E. A. Danso, S. Peräniemi, T. Leiviskä, T. Y. Kim, K. M. Tripathi, A. Bhatnagar, *J. Hazard. Mater.* 2020, **381**, 120871.

22 X. Li, Y. Qi, G. Z. Yue, Y. Li, M. C. Zhang, X. H. Guo, X. F. Li, L. J. Ma, S. J. Li, *Green Chem.* 2019, **21**, 649.

23 S. S, Chen, Y. H. Deng, X. Xiao, S. Xu, P. N. Rudd, J. S. Huang, *Nat. Sustain.* 2021, 1.

24 I. F. Nata, D. R. Wicakso, A. Mirwan, C. Irawan, D. Ramadhani, Ursulla, *J. Environ. Chem. Eng.* 2020, **8**, 104339.

25 Q. Y. Lian, Z. U. Ahmad, D. D. Gang, M. E. Zappi, D. L. Fortela, R. Hernandez, *Chemosphere* 2020, **248**, 126078.

26 Z. L. Li, J. Chen, H. Y. Guo, X. Fan, Z. Wen, M. S. Yeh, C. W. Yu, X. Cao, Z. L. Wang, *Adv. Mater.* 2016, **28**, 2983.

27 A. A. Chavan, H. B. Li, A. Scarpellina, S. Marras, L. Manna, A. Athanassious, D. Fragouli, *ACS Appl. Mater. Interfaces* 2015, **7**, 14778.

28 S. Y. Ding, M. Dong, Y. W. Wang, Y. T. Chen, H. Z. Wang, C. Y. Su, W. Wang, *J. Am. Chem. Soc.* 2016, **138**, 3031.

29 N. Huang, L. P. Zhai, H. Xu, D. L. Jiang, *J. Am. Chem. Soc.* 2017, **139**, 2428.

30 Q. Sun, B. Aguila, J. Perman, L. D. Earl, C. W. Abney, Y. C. Cheng, H. Wei, N. Nguyen, L. Wojtas, S. Q. Ma, *J. Am. Chem. Soc.* 2017, **139**, 2786.

31 D. Zhang, L. Wang, H. H. Zeng, B. Rhimi, C. Y. Wang, *Environ. Sci.: Nano* 2020, **7**, 793.

32 B. L. Chen, L. B. Wang, Y. Q. Xiao, F. R. Fronczek, M. Xue, Y. J. Cui, G. D. Qian, *Angew. Chem. Int. Ed.* 2009, **48**, 500.

33 Y. Z. Jiang, C. Y. Liu, A. S Huang, *ACS Appl. Mater. Interfaces* 2019, **11**, 32186.

34 Y. Hong, D. Thirion, S. Subramanian, M. Yoo, H. Choi, H. Y. Kim, J. F. Stoddart, C. Yavuz, *P. Natl. Acad. Sci. USA*. 2020, **117**, 16174.

35 B. Aguila, Q. Sun, J. A. Perman, L. D. Earl, C. W. Abney, R. Elzein, R. Schlaf, S. Q. Ma, *Adv. Mater.* 2017, **29**, 1700665.

36 T. Wu, C. Liu, B. Kong, J. Sun, Y. J. Gong, K. Liu, J. Xie, A. Pei, Y. Cui, *ACS Cent. Sci.* 2019, **5**, 719.

37 G. W. Yang, H. Y. Han, C. Y. Du, Z. H. Luo, Y. J. Wang, *Polymer* 2010, **51**, 6193.

38 J. M. Chalker, M. Mann, M. J. H. Worthington, L. J. Esdaile, *Org. Mater.* 2021, **3**, 362.

39 J. S. M. Lee, D. J. Parker, A. I. Cooper, T. Hasell, High surface area sulfur-doped microporous carbons from inverse vulcanized polymers. *J. Mater. Chem. A.* 2017, **5**, 18603.

40 J. L. Wang, Y. S. He, J. Yang, *Adv. Mater.* 2015, **27**, 569.

41 H. H. Yuan, C. Guo, J. H. Chen, H. C. Lu, J. Yang, Y. N. Nuli, J. L. Wang, *J. Energy Chem.* 2021, **60**, 360.

42 K. Y. Wang, S. L. Ju, Q. L. Gao, G. L. Xia, G. F. Wang, H. X. Yan, L. X. Dong, Z. X. Yang, X. B. Yu, *J. Alloy Compd.* 2021, **860**, 158445.

43 Y. L. Ren, J. L. Hu, H. X. Zhong, L. Z. Zhang, *J. Alloy Compd.* 2020, **837**, 155498.

44 A. Benítez, D. D. Lecce, G. A. Elia, Á. Caballero, J. Morales, J. Hassoun, *Adv. Mater.* 2018, **11**, 1512.

45 G. X. Li, J. H. Sun, W. P. Hou, S. D. Jiang, Y. Huang, J. X. Geng, *Nat. Commun.*2016, **7**, 1.

46 W. J. Chuang, J. J. Griebel, E. T. Kim, H. Yoon, A. G. Simmonds, H. J. Ji, P. T.Dirlam, R. S. Glass, J. J. Wie, N. A. Nguyen, B. W. Guralnick, J. J. Park, Á. Somogyi, P. Theato, M. E. Mackay, Y. E. Sung, K. Char, J. Pyun, *Nat. Chem.*2013, **5**, 518.

47 S. Y. Wei, L. Ma, K. E. Hendrickson, Z. Y. Tu, L. A. Archer, *J. Am. Chem. Soc.* 2015, **137**, 12143.

48 S. S. Zhang, *Energies* 2014, **7**, 4588.

49 M. M. Abdallah, M. N. Ahmad, G. Walker, J. J. Leahy, W. Kwapinski, *Ind. Eng. Chem. Res.* 2019, **58**, 7296.

50 K. F. Du, S. K. Li, L. S. Zhao, L. Z. Qiao, H. Ai, X. H. Liu, *ACS Sustainable Chem. Eng.* 2018, **6**, 17068.

51 C. Jin, X. Y. Zhang, J. N. Xin, G. F. Liu, J. Chen, G. M. Wu, T. Liu, J. W. Zhang, Z. W. Kong, *Ind. Eng. Chem. Res.* 2018, **57**, 7872.

52 L. Ding, X. B. Luo, P. H. Shao, J. K. Yang, D. Q. Sun, *ACS Sustainable Chem. Eng.*2018, **6**, 8494.

53 B. Zhang, J. Li, D. N. Wang, M. L. Feng, X. Y. Huang, *Inorg. Chem.* 2019, **58**, 4103–4109 (2019).

54 Y. Li, C.Wang, S. J. Ma, H. Y. Zhang, J. J. Ou, Y. M. Wei, M. L. Ye, *ACS Appl. Mater. Interfaces* 2019, **11**, 11706.

55 Z. Yang, H. W. Liu, J. Li, K. Yang, Z. Z. Zhang, F. J. Chen, B. D. Wang, *ACS Appl. Mater. Interfaces* 2020, **12**, 15002.

56 Z. Qu, L. L. Yan, J. F. Xu, M. M. Liu, Z. C. Li, N. Q. Yan, *ACS Appl. Mater. Interf.* 2014, **6**, 18026.

57 X. G. Yu, J. Y. Xie, J. Yang, H. J. Huang, K. Wang, Z. S. Wen, *J. Electroanal. Chem.* 2004, **573**, 121.

58 M. Tipplook, P. Pornaroontham, A. Watthanaphanit, N. Saito, *ACS Appl. Nano Mater.* 2020, **3**, 218.

59 J. X. Wang, X. B. Feng, C. W. N. Aderson, X. Ying, L. H. Shang, *J. Hazard. Mater.* 2012, **221-222**, 1.

60 Y. Fu, Y. Sun, Y. T. Zheng, J. W. Jiang, C. Y. Yang, J. W. Wang, J. S. Hu, *Sep. Purif. Technol.* 2021, **259**, 118112.

61 L. Zhang, J. H. Zhang, X. L. Li, C. J. Wang, A. J. Yu, S. S. Zhang, G. F. Ouyang, Y. Y. Cui, *Appl. Surf. Sci.* 2021, **538**, 148054.

62 W. Qin, G. Y. Qian, H. B. Tao, J. W. Wang, *Funct. Polym.* 2019, **136**, 75.

63 F. H. Shen, J. Liu, D. W. Wu, C. K. Gu, Y. C. Dong, *Ind. Eng. Chem. Res.* 2018, **57**, 7889.

64 X. Y. Chen, D. Y. Chen, N. J. Li, Q. F. Xu, H. Li, J. H. He, J. M. Lu, *ACS Appl. Mater. Interfaces* 2020, **12**, 39227.

65 J. H. Ma, G. Y. Zhou, L. Chu, Y. T. Liu, C. B. Liu, S. L. Luo, Y. F. Wei, *ACS Sustainable Chem. Eng.* 2017, **5**, 843.

66 X. Y. He, T. Zhang, Q. Yue, Y. L. Zhou, H. L. Wang, N. S. Bolan, R. Jiang, D. C. W. Tsang, *Sci. Total Environ.* 2021, **778**, 146116.

67 S. Pavithra, G. Thandapani, S. Sugashini, P. N. Sudha, H. H. Alkhamis, A. F. Alrefaei, M. H. Almutairi, *Chemosphere* 2021, **271**, 129415.

68 H. Cao, P. Yang, T. Ye, M. Yuan, J. S. Yu, X. X. Wu, F. Q. Yin, Y. Li, F. Xu, *Chemosphere* 2021, **278**, 130369.

69 M. Luo, Y. Liu, J. C. Hu, H. Liu, J. L. Li, *ACS Appl. Mater. Interfaces* 2012, **4**, 1813.

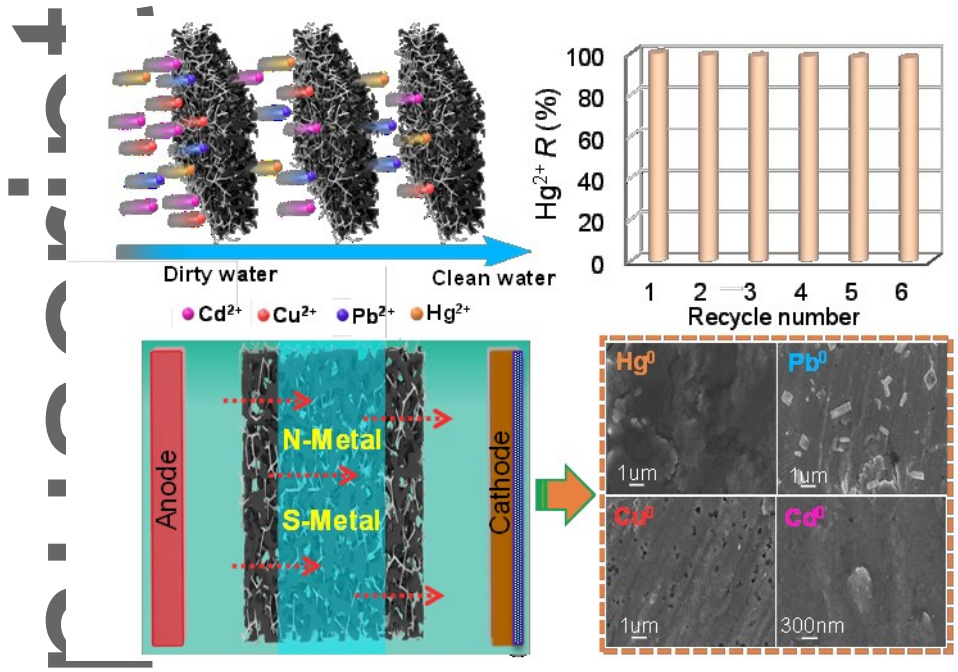

Highly porous and functionalized filter prepared from cyclic π-conjugated backbone and electronic conductivity PAN-S grafted on industrially produced melamine foam. Selective affinity of Hg^{2+}, Pb^{2+}, Cu^{2+}, and Cd^{2+} is achieved. Chemically adsorbed metals ions can be electrochemically desorbed and reduced on counter-electrode, which achieving highest possible waste concentration. Both adsorption and desorption are exceptionally robust. This paradigm offers a sustainable and affordable approach for HMIs recovery from wastewater.